Structural and Rheological Properties of Aqueous Viscoelastic Solutions and Gels of Tripodal Cholamide-Based Self-Assembled Supramolecules

Pierre Terech*,† and Uday Maitra‡

CEA-Grenoble, INAC-SPrAM (UMR5819)-LASSO, 17, rue des Martyrs, 38054 Grenoble Cedex 9, France, and Department of Organic Chemistry, Indian Institute of Science, Bangalore 560 012, India

Received: April 14, 2008; Revised Manuscript Received: August 25, 2008

A tripodal cholic steroid (TCS+) derivative forms hydrogels in acidic conditions that are studied by the small-angle neutron scattering and rheometry techniques. The self-assembled systems exhibit particular scattering and flow properties unusual in the class of molecular gels. The scattering data show separated form- and structure-factor features with, respectively, a low-Q correlation peak and a large-Q secondary oscillation. A probable aggregation model is deduced involving 3 TCS+ molecules per cross-section of fibrillar aggregates packed in a tail-to-tail fashion. The fibers have monodisperse cross-sections (40 Å diameter) and result from a versatile mechanism taking advantage of the free articulation of the three hydrophobic steroid pods ("umbrella-like" packing) around the N+ charge. The N+ charges are distributed at the periphery of the cylinders and give rise to a moderate linear charge density ($\nu \sim 0.16$ e/Å). The variation with concentration of the static scattering structure factor peak $S(Q)$ reveals ordering properties typical of 1d polyelectrolytes. The fibers further organize into fractal clusters characterized by their scattering signature at low-Q and also by the exponent of the scaling of the elastic shear modulus with the concentration. It is suggested that the TCS+ polyion fibers extend under shear (or in a concentrated environment) by varying the angle between the pods along the fiber axis. Viscosity overshoots appear at the startup of shear flow experiments. Analogies with the phenomenology observed with DNA solutions are discussed.

1. Introduction

Self-aggregation of low-mass, ionic amphiphiles in aqueous solutions is known to produce spherical micelles beyond the critical micellar concentration (cmc).[1] In some cases, sphere-to-rod transitions can be induced above a given concentration[2] or by addition of specific cosurfactants.[3−5] A first critical concentration C^* corresponds to the situation where species can no longer diffuse in solution without steric interactions between their neighbors. With unidirectional (1d) rigid species, large aspect ratios (L/D, L being the length and D the diameter of the rods) correspond to low overlap concentrations. Concomitantly, viscoelastic properties appear. At higher concentrations (beyond C^{**}), the increased packing induces ordering of the 1d species into nematic-like phases. Three regimes can thus be defined according to the following set of relations where C is a concentration ([g·cm^{-3}]):

Dilute	$C^* \ll 1/L^3$	
Semi-dilute	$1//L^3 \ll C \ll 1/DL^2$	(1)
Lyotropic (nematic-like)	$C^{**} \gg 1/DL^2$	

Depending on the scission energy of the 1d species and the balance between short-range attractive and long-range repulsive components of the free energy of the systems, a variety of viscoelastic features can be observed. In good solvent conditions, repulsions between the self-assembled species are maximal, and if their scission energy is comparable to the thermal energy kT, scission-recombination kinetic reactions can provide a mechanism for mechanical stress relaxation that is more efficient than the ordinary reptational mode.[6,7] Thus, for highly breakable supramolecules, Maxwell liquids can be obtained. On the other hand, if the scission energy is too large and/or the short-range attraction component has a sufficient strength, the 1d species can merge into junction zones and a 3d percolated network can develop. Such gel-like systems, where the motion of the solid component is restricted in space, present a liquid-to-solid phase transition characterized by a storage modulus and arrested motions of the solidlike aggregates.

The class of molecular gels[8] is made up of supramolecular assemblies associated through physical interactions and contrasts with the covalently reticulated polymeric networks found in chemical gels.[9,10] Molecular gels (hydro- or organo-) can be formed in a large range of liquids at low concentrations ($C =$ 0.01 g·cm^{-3} or less).[11,12] The development of the field is motivated by fundamental challenges associated to the understanding of the following: (i) the hierarchical structural organizations, (ii) the mechanisms of the chirality transduction between the molecular to supramolecular length scales and, (iii) the interactions between the supramolecular assemblies under external stimuli (hydrodynamic fields). The increasing number of applications based on the network properties or on the individual morphologies in replication protocols or the elaboration of functional materials[13,14] also contribute to their interest. For environmental and biological reasons, aqueous systems deserve special attention and in particular, the category of charged 1d species. Although it is known that covalent polymers with ionizable groups can lead to the specific behaviors of polyelectrolytes,[15] differing from those of uncharged polymers, the class of self-assembled polyelectrolytes (SAPEs) carries an

* To whom correspondence should be addressed. Tel: +33 4 38 78 59 98. Fax: +33 4 38 78 56 91. E-mail: pierre.terech@cea.fr.
† CEA-Grenoble, INAC-SPrAM (UMR5819)-LASSO.
‡ Indian Institute of Science.

10.1021/jp803212r CCC: $40.75
Published on Web 10/04/2008

SCHEME 1: Formula of the Tripodal Steroid TCS+ in Aqueous Acetic Acid Solutions[a]

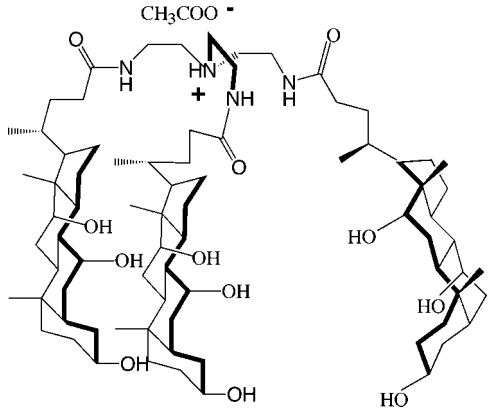

[a] The stoichiometry $C_{80}H_{132}N_4O_{14}D_4$ is assumed for a weak degree of dissociation of the acetate ions.

additional interest in the nonpermanent character of the 1d polyion aggregates. DNA[16] illustrates the importance of biological polyelectrolytes while metallo-supramolecular polymers,[17] among other systems, can represent the synthetic systems as well as the need for a fundamental understanding of SAPEs in view of applications for redox, magnetic, or optical devices. The theoretical context describing the SAPEs is particularly rich and mixes physical concepts of polymers,[18] polyelectrolytes,[15] surfactants[1] and equilibrium polymers[6,19] in solution.

We report on a tripodal cholic steroid (TCS), with nine hydroxyl groups, that forms viscoelastic solutions and thermoreversible molecular hydrogels at very low concentrations (the minimum concentration at which gelation occurs is $C_g \sim 0.0045$ g·cm^{-3}). TCS has three asymmetric steroidal pods coordinated to a protonated nitrogen central atom. Small-angle neutron scattering (SANS) measurements are used to characterize the morphology and sizes of the aggregates. The combination of three features makes the protonated TCS+ system remarkable in the class of molecular gels. First, the charged aggregates exhibit scattering features typical of 1d polyelectrolytes that can be ordered on a micron length scale. Second, the structure of the 1d TCS+ aggregates involves a particular molecular aggregation mechanism ("umbrella-like" packing) taking advantage of the tripodal nature of the TCS+ "monomeric" species so as to form fibers with monodisperse cross-sections. Third, the startup of shear flows exhibits viscosity overshoots preceding a more common shear-thinning behavior.

2. Experimental Section

The synthesis of the nonahydroxy derivative TCS (Scheme 1) and the elementary properties of its hydrogels were formerly described.[20] Solutions and gels were prepared by dissolving TCS into pure acetic acid prior to a dilution in desionized water to the desired concentration. For instance, for a 80:20% v/v CH_3COOH/H_2O mixture and $C_{TCS} = 0.015$ g·cm^{-3}, the final pH is ca. 2.5. Under such pH circumstances, only the central N atom is charged (TCS+) while the three other N atoms, from nonbasic amidic segments are not. Structural properties of the viscoelastic solutions were investigated by SANS experiments at the Institut Laue Langevin (ILL, Grenoble, France) using the large dynamic range small-angle diffractometer D22. Complementary scattering experiments were performed at the European Synchrotron Radiation Facility (ESRF, Grenoble, France, ID01 beamline) and National Institute of Standards and Technology (NIST, Gaithersburg, MD, 30 m beamline). Fully deuterated water and acetic acid were used for neutron scattering to restrict the incoherent scattering to that of the protons of the TCS+ molecules themselves. The isotropic 2d scattering patterns were radially averaged using standard correction procedures.[21] In particular, the subtraction of the incoherent scattering arising mainly from the protons of the TCS+ molecules themselves was made assuming that the aggregates exhibit sharp interfaces with the surrounding liquid phase. The adjustment was then made so that a large-Q intensity decay closest to a Q^{-4} profile was obtained. The range of the scattering vector Q was from 0.001 to 0.6 Å^{-1} where $|Q| = Q = (4\pi \sin\theta)/\lambda$, λ being the neutron wavelength and θ half the scattering angle (λ was 6 and 15 Å). Rheological measurements used a stress-rheometer RS600 (Thermo Electron Corporation) equipped with cone-plate geometries (35 mm diameter, 2° angle and 60 mm diameter, 2° angle). The temperature was regulated to within ±0.1 °C and a cap protected the sample from significant solvent evaporation during the measurements. Optical microcopy investigations using crossed polarizers have been performed with a Olympus BX 100 apparatus and 1 mm quartz cells.

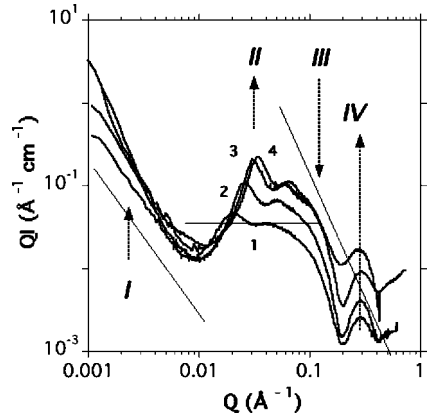

Figure 1. Normalized SANS intensity curves (QI versus Q plots) of TCS+ solutions in deuterated acetic acid/water mixtures (20:80%v/v). (1) $C = 0.0106$ g·cm^{-3}; (2) $C = 0.0205$ g·cm^{-3}; (3) $C = 0.0293$ g·cm^{-3}; (4) $C = 0.0331$ g·cm^{-3}. Four typical scattering features (I, II, III, IV) are identified (see text) by dotted arrows. Three thin full lines are guide lines for −1.8, 0, and −3 slopes of the intensity decay in the Holzer representation (see text).

3. Results and Discussion

3.1. Scattering Properties. Figure 1 shows typical static SANS curves of the TCS+ gel-like systems. The scattering curve is first composed of a sharp intensity decay (feature I) at low-Q values followed by a more "flat" region including a concentration-sensitive peak (feature II) whose apex is at Q_{max}. Then, a second ca. Q^{-4} sharp decay (feature III) is followed by a pronounced intensity oscillation (feature IV) at a Q-value almost independent of the concentration. TCS+ hydrogels can be formed at low concentrations, and it is reasonable to expect that rigid fibrillar aggregates form the network as it is common with molecular gels.[8] Features I, III, and IV are usually observed with molecular gels[22] but feature II is a rare observation for molecular hydrogels. Feature I can be assigned to junction zones of the fibers in the network (vide infra). Indeed, the associated scattering is a sharp intensity decay $Q^{-\beta}$ with $\beta \sim 3$. In ordinary molecular gels, such a contribution exhibits a sharper decay with $\beta = 4$ that can be accounted for by a random two-phase distribution model.[23] In the following, the analysis of this feature will be refined consistently with other length scales of the gel networks and their rheological properties. Interestingly, features

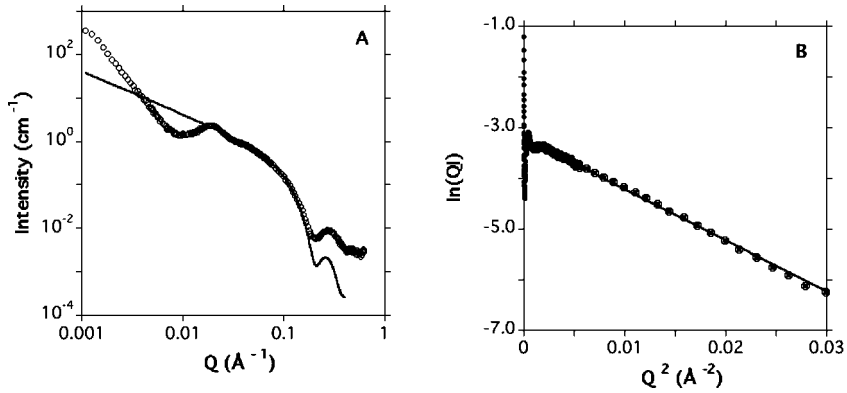

Figure 2. SANS data analysis of TCS+ hydrogels in deuterated acetic acid/water mixtures (20:80% v/v). (A) The full line is a fit using the form-factor function (expression 2) for long and rigid rods with homogeneous cross-sections ($R = 20.0$ Å, $\varepsilon = \Delta R/R = 0.12$) at $C = 0.0106$ g·cm^{-3}. (B) Guinier analysis using expression 2 (straight line) $I = -3.2091 - 100.65\ Q^2$ in the Q-range 0.002−0.0034 Å^{-1} for rods with a cross-sectional radius of gyration ($R_c = 14.2$ Å) at $C = 0.0106$ g·cm^{-3}. In the following, the Guinier analysis is used (expression 3).

III and IV are characteristic features for the existence of 1d aggregates with finite (feature III) and rather monodisperse cross-sectional sizes (feature IV). The scattering function for long, rigid, and cylindrical fibers (expression 2) is used to analyze features III and IV from appropriate Q-expansions.[24] A QI versus Q Holzer representation was chosen in Figure 1 to visualize the flattened region in the intermediary Q-range containing the peak of feature II.

$$I(Q) = \frac{\pi C M_L \Delta b^2_{spec}}{Q}\left[\frac{2J_1(QR)}{(QR)}\right]^2 \qquad (2)$$

with M_L being the molecular weight per unit length of the rodlike aggregate of radius R, Δb^2_{spec} is the specific neutron contrast of the aggregate, and J_1 is the Bessel function of the first kind.

At large Q/R values, expression 1 reduces to lim $I \rightarrow S/Q^4$, a behavior, assimilated to experimental feature III characterizing the interface S of the cylindrical aggregates.[25] Feature IV corresponds to a form-factor oscillation typical of the shape, size, and dispersity of the circular cross-sections as modeled by the Bessel function J_1. Expression 1 also indicates that additional evidence for the existence of linear aggregates is obtained through a Q^{-1} asymptotic decay at low-Q ($1/L_p < Q < 1/R_c$, R_c being the cross-sectional radius of gyration with $R_c = R/\sqrt{2}$, and L_p being the persistence length). The observation of the Q^{-1} decay, located between features II and III, is partially masked by the peak of feature II but still appears as a flatter region in the Holzer representation of Figure 1. The intensity decay in the intermediary Q-range (not including features I and II) follows expression 1, as shown in Figure 2A for cylindrical fibers with $R \sim 20.0$ Å. The general profile is correctly reproduced as well as the Q-position of the form-factor oscillation at $Q \sim 0.27$ Å^{-1} (if an heterogeneous radial contrast profile of the fibers is included, the slight discrepancy in the intensity level of the oscillation would be reduced, not shown). The value of the radius of fibers is confirmed by an independent method using a specific angular domain (Guinier's domain) so that $Q \leq 1/R_c$. In such conditions, a ln(QI) versus Q^2 plot (expression 3) exhibits a linear part from which both the cross-sectional radius and molecular weight per unit length parameters can be extracted. Figure 2B shows such a plot with a slope d(ln(QI))/d$Q^2 = 100.65$ cm^{-1}·Å leading to a radius of gyration $R_c = 14.2$ Å and a geometrical radius $R = 20.0 \pm 1$ Å. In the following, only the Guinier's analysis is used to extract the structural features of the fibers following expression 3.

$$QI = (\pi C M_L \Delta b^2_{spec})\exp - Q^2R_c^2/2 \approx QI_0\left(1 - \frac{R_c^2}{2}Q^2\right) \qquad (3)$$

The 1d TCS+ aggregates appear thin enough to account for a low C_g value at which a percolated network can be obtained. Usually, $C_g > C^*$, since at the overlap threshold, the elasticity may not yet be large enough to ensure a macroscopic gelation phenomenon that is experimentally recognized by an inverted test tube method (e.g., for TCS+ $C_g \sim 0.0045$ g·cm^{-3}). Interestingly, the viscoelastic TCS+ samples can incorporate large amounts of acidic solvent by simple shaking of the specimens. This behavior is unusual in the class of molecular gels[8] and has similarities with suspensions of polymeric chains in good solvent conditions[18] with a weak Flory interaction parameter (or a positive second virial coefficient and stabilizing repulsive interactions). It suggests that entanglements between TCS+ fibers are weak and transient connections accounting for the ability to swell and the existence of feature I in the scattering. This swelling behavior is also encountered in polyelectrolytes and allows the system to decrease its free energy by increasing its volume through an osmotic-driven process. This will be mentioned again in the following to further refine the contours of the most appropriate physical framework.

The origin of the peak (feature II) can now be analyzed in a particular context since the form-factor features III, IV appear well Q-separated from the structure-factor feature II. First, it is known that fibers in molecular gels can be oriented by shear stresses, strong magnetic fields,[26] or through excluded volume interactions; as a result, anisotropic scattering patterns develop with elliptical isointensity contour plots or spots[27] distributed along an equatorial line.[28] The oriented material is then a patchwork of domains and the global order parameter is usually rather poor in comparison with those found with liquid crystals[29] or micellar systems undergoing shear.[30] Indeed, the elastic gel network opposes antagonist restoring stresses to the orientation torques. With TCS+ systems, the scattering is isotropic. Nevertheless, the hypothesis of a system made as a patchwork of microdomains smaller than the irradiated volume cannot be discarded (vide infra). Second, it is known that a suspension of interacting, randomly dispersed spherical and charged scatterers can produce a correlation peak. A suitable modeling can be

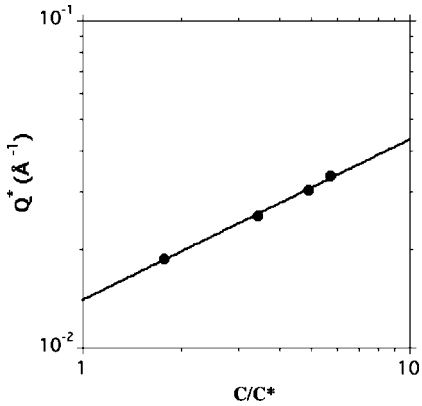

Figure 3. Scaling of the scattering peak position Q_{max} with the concentration. The scaling exponent ca. 1/2 confirms the semidilute regime of the correlated TCS+ fibers.

achieved using a decoupling between the form- and structure- ($S(Q)$) factors based on the Ornstein−Zernike (OZ) equation describing the spatial correlation fluctuations associated to a "closure relationship.[31] In particular, analytical forms for $S(Q)$ as a function of the concentration only including the excluded volume of the spheres can be obtained[32] with the OZ approximation associated to the Percus−Yevick approximation. With TCS+, the situation is more complex since 1d species are characterized by SANS (Figures 2) and consequently, the interaction potential should make $S(Q)$ dependent on the positions of the centers of gravity and the direction of the fibers.[33]

For nonoriented anisotropic scatterers, the structure factor cannot be decoupled from the form-factor and sophisticated approaches are to be considered. Monte-Carlo simulations[34] of the interaction energy can be used to extract a pair distribution function defined as the probability density function for the center of mass distance and the orientations of two fibers. An alternative method models the effective potential between charged rodlike species as the sum of hard spheres and screened Coulomb interactions. For instance, the Polymer Reference Interaction Site Model[35] relates the intermolecular site−site total correlation function to the single chain structure factor. At low concentrations, a liquidlike layering phenomenon appears due to the packing of spheres confining charged chains; consequently, the site−site pair correlation function presents oscillations. The chains are interpenetrating when the concentration is raised since the screening length $1/\kappa$ decreases ($\kappa \sim C^{1/2}$). The interpenetration degree of the spherical envelopes depends on the shape of the "entrapped" scatterers. The actual volume fraction of 1d species inside the envelopes is small compared to that of spherical species and enables a significant interpenetration degree. The liquidlike layering phenomenon with charged rods is then decreasing with increasing concentration while it is increasing with spherical colloids. Thus, polyelectrolyte solutions[15] can present a static structure factor $S(Q)$ at low concentrations with a peak attributed to the liquidlike layering phenomenon on a length scale of the order of the size of the macromolecular species. The peak broadens as the concentration is increased and moves to higher Q indicating a decrease of the ordering.[35] With TCS+ systems, a $c^{1/2}$ scaling of the scattering vector of the first static structure factor maximum is observed following expression 4 (Figure 3), as expected in a system that orders in conditions of screened Coulomb interactions between charged fibers.[36]

$$Q_{max} \sim C^{\upsilon} \tag{4}$$

with $\nu = 1/3$ for dilute solutions and 1/2 for semidilute solutions as illustrated with fd-virus[37] or tobacco mosaic virus[38] solutions and other systems.[36,39] For $C \gg C^*$, the packing orientational entropy dominates the electrostatic repulsion and a hexagonal packing can schematize the situation. It is interesting to note that for rigid rodlike polyelectrolytes, the liquidlike ordering phenomenon and the orientational correlation of the rods can be simultaneous processes that would produce an indistinguishable scattering feature, that is, the correlation peak(s). The effect of concentration upon the width of the first correlation peak should distinguish the two conceptual frameworks for their analysis (vide infra). With TCS+, it can be observed (Figure 1) that a "second-order-like" peak can be distinguished when the concentration is further increased. This feature could be assigned to an enhanced ordering from a poorly structured system ("liquidlike") to a 2d columnar ordering. Such an evolution suggests that C^{**} (relations 1) is reached beyond $C \sim 0.02$ g·cm^{-3}.

For exhaustiveness, it can be mentioned the "correlation hole" theory[18,40] associated with repulsive interactions between charged rods balanced by attractive electrostatic forces through the intermediary of counter-ions. The origin of the peak would then be a correlation hole generated by repulsive interactions between charged rods. The existence of a weak attraction between rodlike macroions has been demonstrated using SAXS.[41] The distribution of the counterions along the radial direction of a rodlike macroion can be calculated with the Poisson−Boltzmann cell model associating Manning's condensation hypotheses.[42,43] The radial (or $Q_\perp$) direction is important for rodlike scatterers since only orientations[25] of Q perpendicular to the rod axis contribute to the intensity. Thus, fluctuations of the number density of counterions along the rod axis can be at the origin of attractive forces between the macroions.[44] Nevertheless, the application of such a model to the TCS+ system is not justified since the scaling of the peak with C and the variation of the peak parameters (position, amplitude, width) are consistent features in a framework involving an anisotropic distribution of the envelopes of the charged scatterers.[23]

$$n_L = \frac{M_L}{M} 10^3 N M_L = \frac{(QI)_0}{\pi M^2 (C - C_g) f \Delta b^2_{spec}} \tag{5}$$

M is the TCS molecular weight, N is Avogadro's number, and f is the fraction of fibers in the network. The driving force for the aggregation phenomenon in molecular gels is known[22] to be the supersaturation degree so that only the excess concentration with respect to a "solubility" limit (e.g., C_g) participates to the growth of 1d aggregates. Such an effective concentration ($C - C_g$) should also be corrected for the bundling processes that ensure the connectivity of the network. The nodal fraction has a scattering signature different from that described by the form-factor expression 2 and contributes differently to the extrapolated value $(QI)_0$ from which n_L values are deduced (expression 3). For the systems under consideration, the nodal fraction is assumed to be negligible ($f \sim 0.99$).

After the characterization of the interaction of the polyionic fibers in solution, it is useful to refine the SANS analysis in accordance with the electrostatic requirements of the TCS+ system. The number of molecules n_L aggregated within a cross-sectional repeating unit along the fiber axis can be extracted from the absolute scattering intensities following a procedure already successfully applied to molecular gels.[45] n_L is related to the molecular weight per unit length according to expression

SCHEME 2: Molecular Aggregation Model (Acetate Ions Are Not Represented)[a]

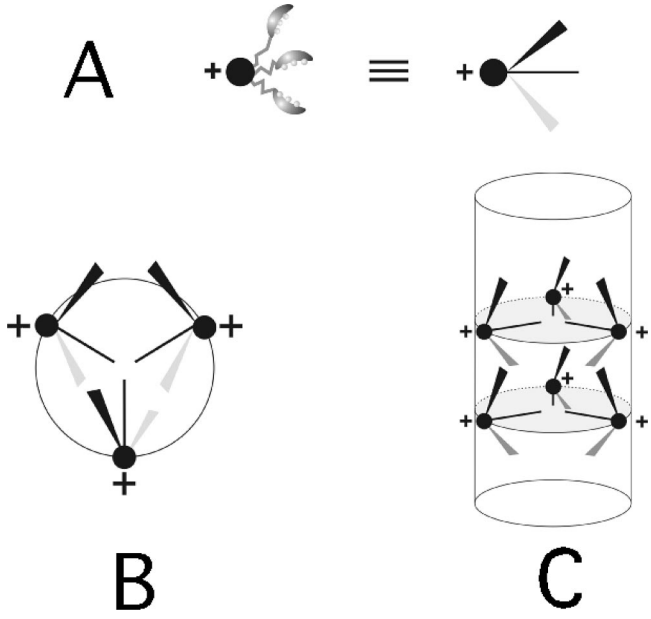

[a] (A) Representation of the tripodal TCS+ molecule. The black sphere is the charged N atom. The facially curved steroid pods are represented as "banana-like" shapes with three spherical OH groups, and the schematized representation is shown on the right. (B) Cross-sectional view showing the three molecules involved per cross-sectional axial repeating unit. The N+ charges are located at the outer cylindrical interface. (C) View of the cylindrical fibers and the distribution of the TCS+ molecules along two cross-sectional layers.

5. The extrapolation at $Q \rightarrow 0$ of $\ln(QI)$ versus Q^2 plots (e.g., Figure 2C) provides the quantity $(QI)_0$ from which n_L can be calculated. To illustrate, at a concentration $C = 0.0106$ g·cm^{-3}, and $C_g \sim 0.0045$ g·cm^{-3} at 20 °C, with a specific neutron scattering contrast value $\Delta b_{spec} = -4.7786 \times 10^{10}$ cm·g^{-1} for TCS+ in a 20:80 CD_3COOD/D_2O mixture, the value $n_L \sim 0.155$ mol·Å^{-1} is found ($C_{80}H_{132}N_4O_{14}D_4$, $(QI)_0 = 0.040392$ Å^{-1} cm^{-1}). Actually, the average value over 10 measurements using two different neutron sources is $n_L \sim 0.165 \pm 0.015$ mol·Å^{-1}. The knowledge of n_L is crucial to decipher the aggregation mechanism at a molecular level. The n_L and R values, experimentally determined through the Guinier analysis, are two structural constraints that direct the modeling options. A reasonable hypothesis assumes that the positively charged nitrogen atoms lie at the external cylindrical interface in aqueous solutions. The mechanism can also take advantage of the extended range of angles that can be potentially adopted by the three hydrophobic pods (length ~ 19 Å, thickness ~ 6−7 Å) to minimize their contacts with the aqueous medium. The significant monodispersity ($\varepsilon = \Delta R/R = 0.12$) of the cross-sections, shown by the resolution of the SANS form-factor oscillation at $Q \sim 0.27$ Å^{-1}, also suggests that the diameter of the TCS+ fibers ($2R = 40$ Å) should compare with the molecular length. The end-to-end distance of the fully extended TCS+ molecule (ca.40 Å) is twice the distance between the positively charged N atom and the end of a pod. Combining these structural parameters, a model can be proposed (Scheme 2) that conciliates the constraints imposed by the optimization of the interactions of the hydrophobic pods in a surrounding aqueous solution, those arising from electrostatic interactions and those related to SANS data. It results that a reasonable model corresponds to a configuration where one of the pods faces another pod of a neighboring molecule in a bimolecular tail-to-tail fashion within the cross-sections of the fibers. The two other pods of a given TCS+ molecule are directed upward or downward the fiber axis by using the free rotations around the quaternary ammonium center. Such a mechanism brings a large adjustability of the axial packing parameter (d_{ax}) in relation to the n_L values and the resulting linear charge densities ν of the fibers. The Bjerrum length λ_B is defined as the minimum distance between charges of a polyion that can be supported by the solvent (in water, $\lambda_B = 7.14$ Å); at distances smaller than λ_B, the counterions would condense on the linear structure. The model can thus be described by the following set of relations where R and the length of a hydrophobic pod l_{pod} are fixed parameters:

$$\begin{aligned} &R = 20.0\,\text{Å} \\ &d_{ax} = 2l_{pod}\cos\delta \qquad \text{with } l_{pod} \approx 19\ \text{Å} \\ &n/d_{ax}n_L = 0.165\ \text{mol·Å}^{-1} \\ &n/d_{ax} = \nu[e\cdot\text{Å}^{-1}] \end{aligned} \tag{6}$$

with n being the number of TCS+ molecules involved per layer along the fiber axis, d_{ax} is the axial repeating unit along the fiber axis, and δ is the angle between the pod direction and the outer interface of the cylindrical fiber.

It comes that $n = 0.165 \times 2\ L_{pod}\cos\delta$ which for $\delta = 45$ degrees gives $d_{ax} = 27$ Å and $n \approx 4$ molecules while for an angle corresponding to a less opened "umbrella", as expected to protect the hydrophobic pods from the highly polar surrounding environment, such as $\delta = 60$ degrees it comes $d_{ax} = 19$ Å and $n \approx 3$ molecules. Scheme 2 is a naive representation of the probable configuration corresponding to $\nu \sim 3/19 \sim 0.16$ e/Å.

Finally, the charge density of the TCS+ polyion is reasonably less than that of the B-DNA reference polyelectrolyte (one of the most highly charged systems with two phosphate groups along the double helix axis $\nu = 2/3.4 \sim 0.6$ e/Å).

As mentioned above, the pods can explore a range of different flexion angles between them due to their free articulation around the positively charged nitrogen atom. There is no positional correlation between the hydrophobic pods from one layer to the other and no associated Bragg peak at large Q. It is expected that such adjustable structural parameter be sensitive to the environmental conditions (vide infra). The minimal free energy of the TCS+ system optimizes the Coulombic repulsions by adjustment of the structural parameters with direct consequences on the scission energy of the polyions. The singular aggregation mechanism might have consequences on the semistatic properties as probed by bulk rheological experiments. Such experiments will also serve to access a more global view of the TCS+ systems at the micron scale.

3.2. Rheological Properties. The TCS+ systems present a shear-viscosity overshoot at the startup of the shear flow followed by a more classical shear-thinning process at higher shear rates. To illustrate, at $C = 0.0265$ g·cm^{-3}, the apparent viscosity passes through a maximum at about 9 times the value at the basis of the bump (Figure 4A). Figure 4B shows shear stress versus shear rate curves illustrating the nonlinear dynamics of the system that exhibit stress overshoots suggesting the existence of metastable states. Dynamical rheology of equilibrated specimens shows profiles (Figure 5A) with $G' > G''$ at all frequencies of the applied stress in the linear regime of deformations ($0.02 < \gamma < 0.03$ for 0.02 g·cm^{-3} $< C <$ 0.05 g·cm^{-3}). Nevertheless, the profiles are not plateaus as expected for soft solids but are sloped. This is evident at low concentration ($C = 0.00457$ g·cm^{-3}) in Figure 5B where the loss modulus

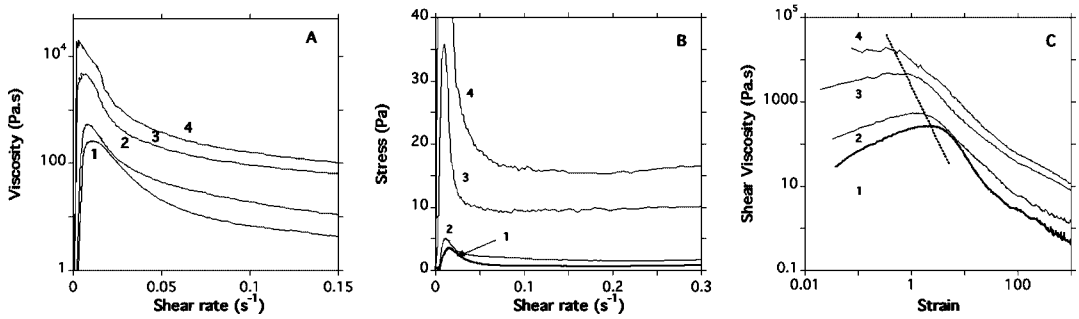

Figure 4. Shear viscosity curves of TCS+ solutions (acetic acid/water 20:80% v/v) show overshoots at the startup of the shear flow: (1) $C = 0.011$ g·cm^{-3}; (2) $C = 0.022$ g·cm^{-3}; (3) $C = 0.033$ g·cm^{-3}; (4) $C = 0.044$ g·cm^{-3}. (A) Viscosity versus shear rate. (B) Viscosity versus strain. The dashed line indicates a dependency of the strain ($\dot{\gamma}t$) with concentration at which the overshoot occurs. (C) Shear stress versus shear rate of the TCS+ hydrogels.

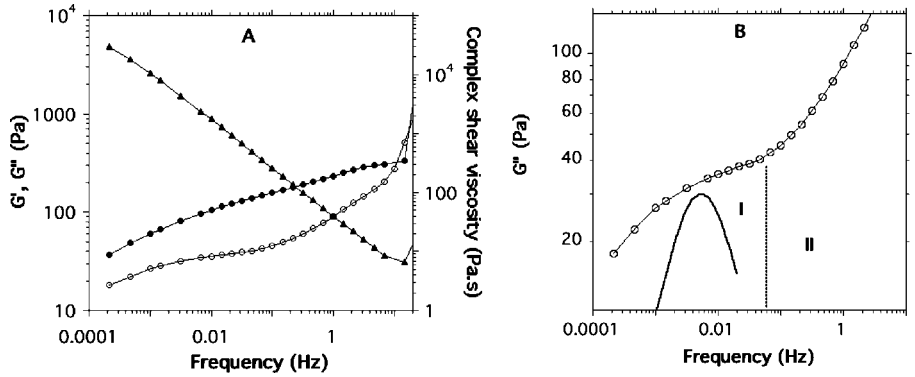

Figure 5. Dynamic rheology of a TCS+ solution ($C = 0.022$ g·cm^{-3}, acetic acid/water 20:80% v/v) at $\sigma = 0.50$ Pa (in the viscoelastic linear regime of strains). (A) Shear modulus G' (●), loss modulus G'' (○), complex shear viscosity η (▲) profiles versus the frequency. (B0 Close-up of the experimental G'' profile. Full line is a Maxwellian mode for $\tau = 29$ s.

profile has a broad bump centered around $\nu \sim 0.0005$ s^{-1} (characteristic time ~ 300 s) indicating that the mechanical relaxation mechanism exhibits a spectrum of slow modes. Such overshoots were never observed with molecular hydrogels that normally behaves as Bingham soft solids with large yield stress values.[46]

The viscosity overshoots arise at startup of shear flows, and the phenomenology should be distinguished from shear-thickening phenomena. Theories[15] have been proposed for shear-thickening of macromolecules with associating groups that can intramolecularly associate and redistribute the associations to intermolecular modes when put in an elongational flow field.[47,48] Such a redistribution of the elastically active segments in the flow field can be observed, for instance, in aqueous solutions of urethane-coupled poly(ethylene oxide) polymers[49] for which the shear thickening is accounted for by a model involving rosettelike micelles with looped chains undergoing a bridge-to-loop transition under shear. With ionomers made of ionic groups attached along a nonpolar chain,[50] the chain elongation in a flow field can increase the ratio between inter- and intrachain associations and can produce shear-thickening. However, in the case of molecular gels, it is known that the constitutive fibers are semirigid or rigid with persistence lengths ranging from a few hundreds of angstroms to several microns: the situation cannot favor the formation of such flexible transient micellar structures.

With self-assembled supramolecules and in particular with breakable wormlike micelles, a shear-induced increase of viscosity can result from a shear-induced phase transition.[51] The phenomenon develops through inhomogeneous nucleation mechanisms at a concentration-dependent shear rate. The steady state behavior is controlled by the shear stress and occurs in low-concentration wormlike micellar systems in a regime where a non-Maxwellian stress relaxation prevails (by contrast to the situation at higher concentrations where the Maxwellian relaxation dominates). It has also been reported that at elevated values of shear stresses or deformations, such systems can exhibit stress overshoots in the startup of shear experiments that can be partly approached by the Giesekus's model.[52] The transition toward shear-induced viscous states can also be continuous as shown with cetyltrimethylammonium tosylate aqueous solutions.[53] In this latter system, a scattering correlation peak due to electrostatic repulsions and a shear-induced increase of viscosity regime strongly depends on temperature but weakly on concentration.[54] The thickening transition was then assumed to couple two states energetically close to each other: a dispersion of chains and a viscoelastic solution of entangled equilibrium polymers. With TCS+ systems, Figure 5 shows that the G'' profile, despite presenting some poor reminiscence, is far from the quadratic variation expected for a Maxwellian function ($G'' = G_0\omega\tau/(1 + \omega^2\tau^2)$, $\omega = 2\pi\nu$). The observation of a Maxwell flow is a rare event with molecular gels where an intrinsic conflict exists since increasing the concentration should increase the frequency of scissions of the fibers but also simultaneously increases the fraction of nodes with large lifetimes.[8,55,56]

The viscosity overshoot observed in the startup of flow of a TCS+ viscoelastic solution is a transient behavior that can be related to the shear-sensitivity of the TCS+ fibrillar morphology built via the particular "umbrella-like" packing mode. The TCS+ polyions (Scheme 2) exhibit an adjustable architecture, and in particular angular adjustments between two pods of neighboring TCS+ molecules along the fiber axis that can generate elongational modes and associated diameter fluctuations. The fiber extension mechanism accounts for the onset of

viscosity overshoots of flow curves. Expressions 5 have shown that a reasonable option for the aggregation mechanism can be the implication of 3 molecules per cross-sectional layer with a spacing d_{ax} between N+ charges along the fiber axis of ca. 19 Å. This distance can easily become larger at the maximum of the viscosity overshoot while $<L>$ increases and R slightly decreases as a consequence of a decrease of the angle δ under shear. The counterion (CH_3COO^-) distribution and its degree of condensation onto the polyion can also be shear-sensitive and participate to the amplitude of the stretching mode under shear flows. Apart from the effect of shear, the confinement in concentrated solutions provided by surrounding tubes of entangled and neighboring TCS+ polyions might also generate fiber elongation modes. At rest, the topological constraints due to the neighboring fibers affect the angles between the interfacial pods and lead to a decrease of the diameters and increase of the contour lengths (and in turn account for the viscosity overshoots). Thus, at $C_0 = 0.0293$ g·cm^{-3}(instead of 0.0106 g·cm^{-3}), the radius of the best fit (not shown) using expression 2 (as for Figure 2A) is $R = 17.0$ Å (instead of 20.0 Å).

It is interesting to observe that the scattering and rheological phenomenologies of the **TCS+** systems exhibit similarities with those for the dynamics of dilute and semidilute DNA solutions both in the steady and startup of shear flows.[57] Single-molecule fluorescence microscopy was used to follow the conformational dynamics of single DNA molecules in the flow while the macroscopic behavior was analyzed with bulk shear viscosity measurements. DNA solutions exhibit a viscosity overshoot preceding that in molecular extension that was found independent of the concentration on both sides of C^* (indicating that the process is not related to the connectivity of transient networks formed beyond C^*). Calculations[57] of the transient shear dynamics, supported by rheology and fluorescence experiments, lead to a prediction of the maximum of shear viscosity at $\dot{\gamma}t \approx 10$. The apex corresponds to the initial alignment and chain extension in the gradient direction at which the chain thickness starts decreasing. The overshoot of shear viscosity at high $\dot{\gamma}t$ values (t being the relaxation time of the polymeric chain) was related to the nonaffine motion of the chain and its thickness decrease. As shown above, the flow behavior of TCS+ solutions exhibits similarities with DNA solutions in the startup of shear flows. Figure 4C shows that the overshoot occurs approximately at a strain in the range $0.5 < (\dot{\gamma}t) < 3$ for concentrations in the range 0.01 g·cm^{-3} < C < 0.04 g·cm^{-3} (a behavior similar to that for DNA). Similarly, it can be envisioned that the viscosity overshoot of TCS+ solutions is related to a fiber extension process facilitated by the particular "umbrella-like" aggregation mode that offers the required angular flexibility between the trimeric TCS+ repeating units along the fiber axis. Nevertheless, the slight dependency of the strain value at the overshoot with the concentration (see Figure 4C) indicates that connectivity effects moderatly intervene in the mechanism. Being aware that the theoretical scaling laws of the viscosity with concentration are established in the zero-shear limit, it can still be instructive to analyze the variation of the viscosity at the maximum of the overshoot. It appears that two apparent regimes of scaling laws (Figure 6) appear. The exponent 1.2 of the first regime compares correctly with the theoretical one (3/2) expected for entangled polyelectrolytes[15] while the second exponent 4.0 (at large concentrations) is consistent with the one for entangled neutral polymer (i.e., 15/4).[18] Despite, the scaling exponents are determined at low-shear rates corresponding to the maximum of fiber elongation, it is intriguing that their order of magnitude remains in the vicinity of the theoretical ones. It

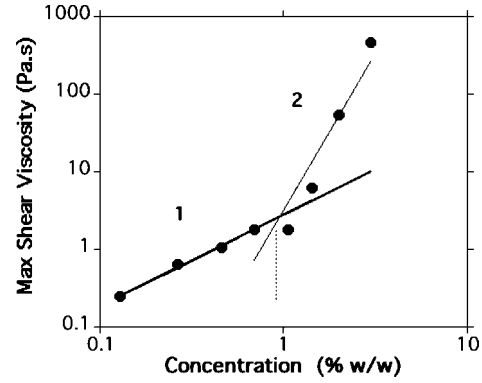

Figure 6. Scaling laws of the shear viscosity at the maximum of the overshoot versus C. Two regimes can be discerned (1, exponent = 1.2; 2, exponent = 4.0).

can be speculated that such observation, expected for polyelectrolytes in a concentration regime beyond the overlap of the electrostatic blobs (where the electrostatic interactions are much less important) so that a quasi-neutral regime is observed[15,58] can be also valid for the TCS+ system. The concentration range of quasi-screened Coulombic interactions in the semidilute regime would thus be reached as already supported by the scaling $Q_{max} \sim C^{1/2}$ of the scattering peak (vide supra).

4. Conclusions

A protonated tripodal cholic acid derivative (TCS+) forms viscoelastic solutions and thermoreversible molecular hydrogels at very low concentrations ($C_g \sim 0.0045$ g·cm^{-3}) whose structural and rheological properties have been investigated. The scattering data provide a consistent structural model of the self-assembled fibers taking advantage of the tripodal nature of TCS+ that involves a trimeric association of the TCS+ molecules per cross-sectional repeating unit (of 40.0 Å diameter) along the fiber axis. The specific molecular architecture offers a capacity for fiber elongation associated to a thickness decrease under shear flow. The axial spacing can be adjusted by a shear-induced (or concentration-induced) variation of the angle between the pods of neighboring molecules along the outer cylindrical interface. A shear-induced viscosity overshoot displayed at the startup of the flow curves can be accounted for by a fiber elongation mechanism. It is observed that the rheological phenomenology of the TCS+ polyelectrolyte solutions and gels is similar to that of DNA solutions.[57] Moreover, the model offers layered hydrophobic environments (where fluorescent hydrophobic probes can accommodate) that are buried along the fiber axis in between the interfacial N+ charges (Scheme 2). This capacity has been previously used to follow the time dependence of the fluorescence during the gelation phenomenon.[20]

The TCS+ system combines properties of ordinary molecular gels and polyelectrolyte systems. Part of the properties is clearly atypical of molecular gels (namely the swelling ability driven by the osmotic pressure and the occurrence of a scattering structure factor peak characteristic of correlations at large distances) but other properties can be encountered only with molecular or colloidal gels (e.g., scaling laws of the elastic moduli). We focused here on the structural features at the nanoscale of the TCS+ fibers and the particular "umbrella-like" packing mode that can be at the origin of fiber extension at the startup of shear flow experiments generating viscosity overshoots. Nevertheless, it is also interesting to consider a more global view of the TCS+

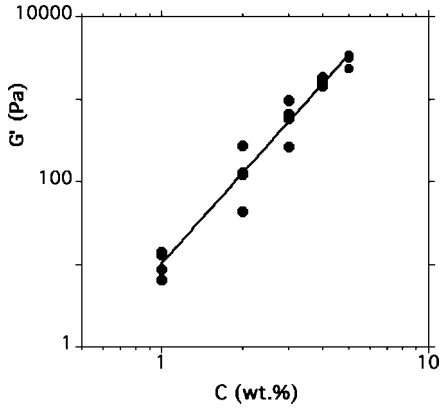

Figure 7. Scaling law ($G' = 9.9C^{3.6}$) of the storage modulus G' (Pa) with the TCS+ concentration in acidic aqueous solutions (acetic acid/water 20:80% v/v).

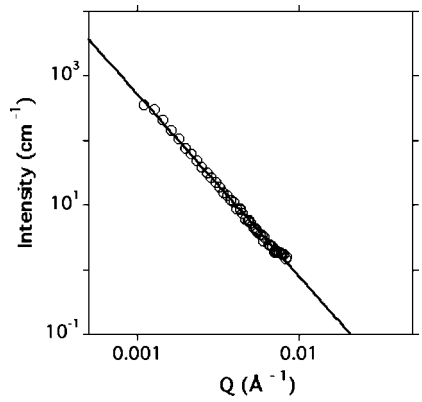

Figure 8. The extra-intensity at low-Q, due to the clustering of TCS+ fibers, follows a $Q^{-2.8}$ decay profile. Example of a hydrogel at C = 0.0106 g·cm^{-3} in the mixture acetic acid/water 20:80% v/v.

systems by analyzing the scaling laws of the elastic shear modulus $G' \propto C^{\alpha}$. With ordinary molecular gels behaving as Bingham solids with no swelling ability, the exponent α is usually of the order of 2.0. Such systems can be described[46,59] as architectures built with rigid fibers rigidly connected in junction zones that are frequently crystalline microdomains. Such networks are purely energetic and can be deformed only by bending its fibers. Figure 7 shows that the experimental scaling behavior of the storage modulus of TCS+ hydrogels exhibit a much larger exponent $\alpha = 3.6$. If some entropy is introduced by allowing some degree of rotational freedom in the junction zones, a moderate decrease of the exponent α is expected and such a context cannot thus be suitable for the description of the TCS+ systems. On the other hand, scaling theories[60,61] for the modulus G' of polyelectrolyte gels as a function of salt content and solvent quality are available. To summarize, the configuration of a 1d polyelectrolyte in a semidilute solution with added salt exhibits different length scales such as the size of the electrostatic blobs, the correlation length of the semidilute regime and the electrostatic screening length. The elasticity of a polyelectrolyte gels cannot be reduced to that of the polyelectrolyte solution due to the influence of the counterion pressure. The shear modulus is then proportional to the elastic energy density and, depending on the various theoretical assumptions that can be made (degree of swelling, affine deformation, stretching degree), the scaling laws exhibit exponents $\alpha < 1$ that also cannot describe the behavior of **TCS+** gels. Finally, the TCS+ systems can also be viewed as colloidal gels involving floclike elements. Depending upon the relative strength of the inter- and intrafloc links, two regimes of elasticity of the gels can be discerned.[62,63] In the weak-link regime, the elasticity of the interfloc links determines the elasticity of the gel, the flocs being more rigid than their connections. The scaling exponent can then be deduced from expression 7

$$\alpha = 1/(d - d_f) \tag{7}$$

where d is the Euclidean dimension of the system and d_f the fractal dimension of the floc. For $\alpha = 3.6$ and $d = 3$, $d_f = 2.7$. The TCS+ flocs would be rather compact clusters of fibers that compartmentalize the liquid volume in which a weak correlation between the 1d charged scatterers develops. The scattering technique is appropriate to characterize such fractal[64] system if the spatial range where the self-similarity relationship applies, is covered by the experimental Q-range. The scattering law is then simply given by relation 8

$$S(Q) \sim Q^{-df} \tag{8}$$

Figure 8 shows the innermost part of the scattering curve in a log−log representation. The intensity decay follows a scaling law (expression 6) with $d_f = 2.8$. The result is in good agreement with the fractal dimension ($d_f = 2.7$) of the clusters deduced from the scaling of the elastic shear modulus. Such a consistency with a model of interacting flocs, which can be more or less swollen and ordered, is also compatible with the unusual (in the class of molecular gels) swelling ability of the system. Interestingly, it has been recently proposed to describe the growth of the type of fractal pattern found in certain organogels by a noncrystallographic branching mechanism occurring via self-mismatch nucleation and growth processes.[65] Thus, with a *N*-lauroyl-L-glutamic acid−based organogelator, a combination of techniques (rheology, static light scattering, and coupled supercritical fluid CO_2 extraction/scanning electron microscopy) was used to extract a fractal dimension $d_f \sim 2.4$. To further describe the ordering within the clusters, corresponding to the scattering feature II, optical microscopy views between crossed polarizers of TCS+ specimens can be commented (Figure 9). The average size of the slightly birefringent domains can be estimated to be of the order of a micron. The irradiated area of specimen by the neutron beam (of the order of 1 cm^2) is much larger than the cluster size and averages the slightly anisotropic domains to provide a resulting isotropic signal. Indeed, the low-Q limit imposed by the SANS setup is ca. 0.001 Å^{-1} (Figure 8) corresponding to correlation distances of a few thousands of Angströms (fractions of microns). The lowest Q-limit, corresponding to the cutoff of the fractality at large distances, is not yet reached and thus it can be assumed that optical observations are related to the fractal collection of clusters entrapping the slightly ordered TCS+ supramolecular polyelectrolytes.

To conclude, the description of the TCS+ hydrogels extends from the molecular level at which the aggregation presents a particular "umbrella-like" packing mechanism (responsible for viscosity overshoots at startup flows), to the nanoscopic scale, as probed by scattering experiments, with evidence for a ordering of the 1d polyelectrolytes and finally to the fractal organization of the clusters at a micron scale with a resulting macroscopic elasticity typical of colloidal gels.

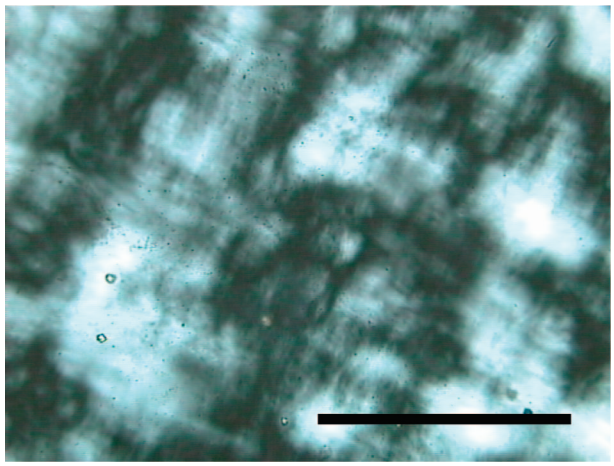

Figure 9. Slightly birefringent domains develop in the gap of two glass cover slides (scale bar is 10 μm, $C = 0.0106$ g·cm^{-3} in a deuterated acetic acid/water mixture 20:80% v/v).

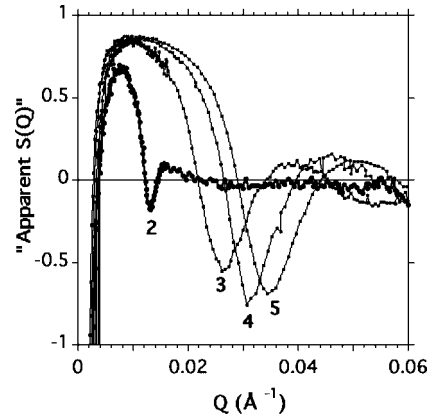

Figure 10. Apparent structure factor extracted as $S(Q)_{app} = 1 - I(Q)_{exp}/P(Q)_{fit}$. $P(Q)_{fit}$ is the fit using expression 1 with $R = 20.0$ Å and $\varepsilon = \Delta R/R = 0.12$. (1) $C = 0.0106$ g·cm^{-3}; (2) $C = 0.0205$ g·cm^{-3}; (3) $C = 0.0293$ g·cm^{-3}; (4) $C = 0.0331$ g·cm^{-3}.

Acknowledgment. The present work was supported by the Indo-French Center for Promotion of Advanced Research (IFCPAR Project 2605-1), which is thanked. Institut Laue Langevin (ILL, Grenoble, France) is acknowledged for providing access to the spectrometer and all technical support. Dr. Bruno Demé (ILL) is acknowledged for his valuable help. Dr. N. Sangeetha (IISc) and G. Galgali are thanked for their help in the preparation of certain samples.

Appendix

A fortuitous decoupling between the scattering structure factor $S(Q)$ and the form factor $F(Q)$ features is experimentally observed (Figures 1,2) that incites to extract a raw estimation of $S(Q)^{app}$ assuming an isotropic interaction potential between the scatterers despite TCS+ polyions cannot be considered as charged pointlike species. $S(Q)$ can be evaluated by the renormalized Hayter-Penfold procedure[31,66] and positional correlations can be given by expression 9

$$I(Q) = n(|\langle F(Q)\rangle|^2 S(Q) + \langle |F(Q)|^2\rangle - |\langle F(Q)\rangle|^2) \quad (9)$$

where $< >$ is an average over all orientations of the rods of number density n.

Interestingly, if the approximation $|\langle F(Q)\rangle^2| \approx |\langle F(Q)\rangle|^2$ is made, the oscillating profile of apparent $S(Q)^{app}$ (Figure 10) is similar to that expected for an ordered liquidlike system. Interestingly, a second order of the correlation peak can be discerned that indicates a significant ordering degree of the TCS+ 1d scatterers and their liquid envelopes.

A simple calculation can illustrate the consistency of the analytical approach. At a concentration $C = 0.0106$ g·cm^{-3}, a first maximum at $Q_{max} \sim 0.0186$ Å^{-1} is observed that would correspond to a mean interaction distance of $\xi \sim 340$ Å, theoretically scaling as $\xi = 2\pi/Q_{max} = R(\pi\rho/C)^{0.5}$ (ρ being the density ([g·cm^{-3}]) of the solid component). Assuming $R = 20.0$ Å, $\rho \sim 1.2$ g·cm^{-3}, C is deduced to be 0.0133 g·cm^{-3} in an acceptable agreement with the experimental value C (0.0106 g·cm^{-3}).

The shape, broadness, and positions of the secondary maxima of the $S(Q)^{app}$ profiles vary as a function of the concentration. The peak clearly broadens and is shifted toward higher Q-values with the concentration as expected in the ordering hypothesis of 1d polyelectrolytes. It is known that in a mean-field thermodynamic approach,[6] the average contour length $<L>$ of wormlike polyelectrolyte chains follows an exponential distribution (expression 10) in the semidilute regime.

$$\langle L\rangle \approx C^{1/2} \exp\left[\frac{1}{2k_B T}(E_c - E_e)\right] \quad (10)$$

E_c is the end cap energy required for generating two end caps, E_e is the effective electrostatic contribution that favors the breaking of the polyion chains, and k_B is the Bolztman constant. E_e depends on the effective charge per unit length while the ionization degree of the chains is affected by the Debye length of the system. The elongation/thinning mechanism of the TCS+ fibers should thus reduce the contribution of the electrostatic term and amplifies the increase of their length by raising the concentration. This is qualitatively in accordance with the existence of a second regime in the scaling law of the viscosity with C exhibiting an increased slope (Figure 6) and also with the enhanced exponent of the scaling law of the shear modulus (Figure 7).

References and Notes

(1) Israelachvili, J. N. *Intermolecular and surface forces*, 3rd edition; Academic Press: London, 1992.
(2) Mackintosh, F.; Safran, S. A.; Pincus, P. A. *Europhys. Lett.* **1990**, *12*, 697–702.
(3) Schurtenberger, P.; Scartazzini, R.; Luisi, P. L. *Rheol. Acta* **1989**, *28*, 372–381.
(4) Shchipunov, Y. A.; Hoffmann, H. *Langmuir* **1998**, *14*, 6350–6360.
(5) Lin, Z.; Cai, J. J.; Scriven, L. E.; Davis, H. T. *J. Phys. Chem.* **1994**, *98*, 5984–5993.
(6) Cates, M. E.; Candau, S. J. *J. Phys.: Condens. Matter* **1990**, *2*, 6869–6892.
(7) Turner, M. S.; Cates, M. E. *J. Phys. II* **1992**, *2*, 503–519.
(8) *Molecular Gels: Materials with Self-Assembled Fibrillar Networks*; Weiss, R. G.; Terech, P., Eds.; Springer: Dordrecht, The Netherlands, 2006, p 976.
(9) Tanaka, T. *Scientific American*, January, 1981, pp 110−123.
(10) Osada, Y.; Khokhlov, A. R. *Polymer gels and networks*; CRC Press: Boca Raton, 2001.
(11) Abdallah, D. J.; Weiss, R. G. *Adv. Mater.* **2000**, *12*, 1237–1247.
(12) Terech, P. Low-molecular weight organogelators. In *Specialist surfactants*; D. R. I., Ed.; Chapman & Hall: London, 1997; Chapter*8*, pp 208−268.
(13) Sangeetha, N. M.; Maitra, U. *Chem. Soc. Rev.* **2005**, *34*, 821–836.
(14) Bong, D. T.; Clark, T. D.; Granja, J. R.; Ghadiri, M. R. *Angew. Chem., Int. Ed.* **2001**, *40*, 988–1011.
(15) Dobrynin, A. V.; Rubinstein, M. *Prog. Polym. Sci.* **2005**, *30*, 1049–1118.

(16) Bloomfield, V. A. In *Nucleic acids structures, properties and functions*; Bloomfield, V. A.; Crothers, D. M.; Tinocco, I., Eds.; University Science Books: Sausalito, CA, 2000; pp 475−528.
(17) Kurth, D. G.; Higuchi, M. *Soft Matter* **2006**, *2*, 915–927.
(18) De Gennes, P. G. *Scaling Concepts in Polymer Physics*; Cornell University Press: Ithaca, NY, 1979.
(19) *Supramolecular Polymers*; Ciferri, A., Ed.; Taylor & Francis: London, 2005.
(20) Maitra, U.; Mukhopadhyay, S.; Sarkar, A.; Rao, P.; Indi, S. S. *Angew. Chem., Int. Ed.* **2001**, *40*, 2281–2283.
(21) (a) http://www.ncnr.nist.gov/. (b) http://www.ill.fr/.
(22) Terech, P.; Weiss, R. G. *Chem. Rev.* **1997**, *97*, 3133–3159.
(23) Debye, P.; Bueche, A. M. *J. Appl. Phys.* **1949**, *20*, 518.
(24) Glatter, O.; Kratky, O. *Small Angle X-ray Scattering*; Academic Press: London, 1982.
(25) Guinier, A.; Fournet, G. *Small Angle Scattering of X-rays*; Wiley: New York, 1955.
(26) Terech, P.; Berthet, C. *J. Phys. Chem.* **1988**, *92*, 4269–4272.
(27) Terech, P.; Jean, B.; Ne, F. *Adv. Mater.* **2006**, *18*, 1571–1574.
(28) Vainshtein, B. K. *Diffraction of X-rays by chain molecules*; Elsevier: Amsterdam, 1966.
(29) Kekicheff, P.; Cabane, C. *Acta Crystallogr.* **1988**, *44*, 395–406.
(30) Penfold, J. *J. Appl. Crystallogr.* **1988**, *21*, 770–776.
(31) Hayter, J. B.; Penfold, J. *Mol. Phys.* **1981**, *42*, 109–118.
(32) Kinning, D. J.; Thomas, E. L. *Macromolecules* **1984**, *17*, 1712–1718.
(33) Maier, E. E.; Krause, R.; Deggelmann, M.; Hagenbuchle, M.; Weber, R. *Macromolecules* **1992**, *25*, 1125–1133.
(34) Schneider, J.; Karrer, D.; Dhont, J. K. G.; Klein, R. *J. Chem. Phys.* **1987**, *87*, 3008–3015.
(35) Yethiraj, A.; Shew, C.-Y. *Phys. Rev. E* **1996**, *77*, 3937–3940.
(36) Matsuoka, H.; Ise, N.; Okubo, T.; Kunugi, S.; Tomiyama, H.; Yoshikawa, Y. *J. Chem. Phys.* **1985**, *83*, 378–387.
(37) Hagenbuchle, M.; Weyerich, B.; Degglmann, M.; Graf, C.; Krause, R.; Maier, E. E.; Schulz, S. F.; Klein, R.; Weber, R. *Physica A* **1990**, *169*, 29–41.
(38) Maier, E. E.; Schulz, S. F.; Weber, R. *Macromolecules* **1988**, *21*, 1544.
(39) Weyerich, B.; D'aguanno, B.; Canessa, E.; Klein, R. *Faraday Discuss. Chem. Soc.* **1990**, *90*, 245–259.
(40) Benmouna, M.; Weill, G.; Benoit, H. *J. Phys. (Paris)* **1982**, *43*, 1679–1685.
(41) Guilleaume, B.; Blaul, J.; Ballauff, M.; Wittemann, M.; Rehahn, M.; Goerigk, G. *Eur. Phys. J. E* **2002**, *8*, 299–309.
(42) Le Bret, M.; Zimm, B. H. *Biopolymers* **1984**, *23*, 271–285.
(43) Le Bret, M.; Zimm, B. *Biopolymers* **1984**, *23*, 287–312.
(44) Ha, B. Y.; Liu, A. J. *Phys. Rev. E* **1998**, *58*, 6281–6286.
(45) Terech, P.; Ramasseul, R.; Volino, F. *J. Phys. (Paris)* **1985**, *46*, 895–903.
(46) Terech, P.; Pasquier, D.; Bordas, V.; Rossat, C. *Langmuir* **2000**, *16*, 4485–4494.
(47) Ballard, M. J.; Buscall, R.; Waite, F. A. *Polymer* **1988**, *29*, 1287–1293.
(48) Tam, K. C.; Jenkins, R. D.; Winnik, M. A.; Bassett, D. R. *Macromolecules* **1998**, *31*, 4149–4159.
(49) Yekta, A.; Xu, B.; Duhamel, J.; Adiwidjaja, H.; Winnik, M. A. *Macromolecules* **1995**, *28*, 956–966.
(50) Witten, T. A.; Cohen, M. H. *Macromolecules* **1985**, *18*, 1915–1918.
(51) Hu, Y. T.; Boltenhagen, P. *J. Rheol.* **1998**, *42*, 1185–1208.
(52) Fisher, P.; Rehage, H. *Rheol. Acta* **1997**, *36*, 13–27.
(53) Gamez-Corrales, R.; Berret, J.-F.; Walker, L. M.; Oberdisse, J. *Langmuir* **1999**, *15*, 6755–6763.
(54) Berret, J.-F.; Gamez-Corrales, R.; Oberdisse, J.; Walker, L. M.; Lindner, P. *Europhys. Lett.* **1998**, *41*, 677–682.
(55) Berret, J. F.; Appell, J.; Porte, G. *Langmuir* **1993**, *9*, 2851–2854.
(56) Terech, P.; Coutin, P. *J. Phys. Chem. B* **2001**, *105*, 5670–5676.
(57) Hur, J. S.; Shaqfeh, E. S. G.; Babcock, H. P.; Smith, D. E.; Chu, S. *J. Rheol.* **2001**, *45*, 421–450.
(58) Dobrynin, A. V.; Colby, R. H.; Rubinstein, M. *Macromolecules* **1995**, *28*, 1859–1871.
(59) Jones, J. L.; Marques, C. M. *J. Phys. (Paris)* **1990**, *51*, 1113–1127.
(60) Rubinstein, M.; Colby, R. H.; Dobrynin, A. V.; Joanny, J. F. *Macromolecules* **1996**, *29*, 398–406.
(61) Vilgis, T. A.; Johner, A.; Joanny, J. F. *Eur. Phys. J. E* **2000**, *3*, 237–244.
(62) Shih, W.-H.; Shih, W. Y.; Kim, S.-I.; Liu, J.; Aksay, I. A. *Phys. Rev. A* **1990**, *42*, 4772–4779.
(63) Wu, H.; Morbidelli, M. *Langmuir* **2001**, *17*, 1030–1036.
(64) Teixeira, J. *J. Appl. Crystallogr.* **1988**, *21*, 781–785.
(65) Liu, X. Y.; Sawant, P. D. *Appl. Phys. Lett.* **2001**, *79*, 3518–3520.
(66) Hansen, J. P.; Hayter, J. B. *Mol. Phys.* **1982**, *46*, 651–656.

JP803212R